SOILS AND FOUNDATIONS Vol. 31, No. 2, 164-174, June. 1991
Japanese Society of Soil Mechanics and Foundation Engineering

ON THE CONCEPT OF CHARACTERISTIC STATES OF COHESIONLESS SOIL AND CONSTITUTIVE MODELING

M. OMAR FARUQUE[1] and M. MUSHARRAF ZAMAN[1]

ABSTRACT

The concepts of two characteristic states and their representation as characteristic state lines in the stress space are introduced to describe volumetric behavior of cohesionless soil during shearing. The first characteristic state line represents the state of cohesionless soil at failure, while the second characteristic line represents the state at which the rate of volumetric strain momentarily vanishes as the soil passes from the compressive mode of deformation to the dilative mode of deformation during shearing. Explicit forms of the two characteristic state lines in the stress space are proposed and used to develop a constitutive model based on the framework of plasticity theory. The general forms of the characteristic state lines are verified using drained shear test data for a fine sand. Stress-strain and volumetric-axial strain responses are predicted using the proposed model and good correlations are observed with experimental data.

Key words: characteristic states, cohesionless soil, constitutive model, dilatancy, elasticity, plasticity, volumetric response (**IGC**: D/0)

INTRODUCTION

Numerical methods such as finite element and boundary element are used frequently to analyze geotechnical engineering problems under static and dynamic loadings. As solution tools, these numerical techniques are extremely powerful and can be used for the analysis of many geotechnical engineering problems involving soil whose solutions are intractable otherwise. However, use of sophisticated numerical techniques do not always guarantee useful practical solution of such problems. One of the main reasons for this is the use of constitutive models that are deficient in describing the stress-strain and volumetric response of soils.

Many constitutive models have been developed in the past for cohesionless soil using the framework of plasticity theory [1 - 13, 15, 17, 19, 20, 22, 23, 25, 26, 28 - 31]. A majority of these models emphasize on the characterization of stress-strain response and do not adequately address the volumetric behavior. Consequently, predicted volumetric response exhibits substantial deviation from experimental observation than the predicted stress-strain response. For cohesionless soil, characterization

[1] School of Civil Engineering and Environmental Science, University of Oklahoma, Norman, OK 73019, USA.
Manuscript was received for review on April 20, 1990.
Written discussions on this paper should be submitted before January 1, 1992, to the Japanese Society of Soil Mechanics and Foundation Engineering, Sugayama Bldg. 4F, Kanda Awaji-cho 2-23, Chiyoda-ku, Tokyo 101, Japan. Upon request the closing date may be extended one month.

of volumetric response is of particular importance because such soil can undergo significant volume change during shearing.

The concepts of characteristic states and their representation as characteristic state lines in the stress space are introduced to describe volumetric behavior of cohesionless soil during shearing. Explicit forms of the characteristic state lines in the stress space are proposed and used to develop a constitutive model based on the framework of plasticity theory. The general forms of the characteristic state lines proposed are verified using drained shear test data for a fine sand. Stress–strain and volumetric-axial strain responses are predicted using the proposed model and good correlations are observed with experimental data.

THE CHARACTERISTIC STATES OF COHESIONLESS SOIL

Past experimental investigations on cohesionless soil have revealed two characteristic states in its stress–strain response during shearing (Fig. 1) [1, 2, 6, 13, 14, 16, 19, 21]. One of these characteristic states (e. g., point 1 in Figs. la and lb) is attained as the soil approaches the state of failure. In this state the soil experiences progressive shear deformation under constant volume (i. e. zero rate of volumetric strain). The second characteristic state (e. g., point 2 in Figs. 1(a) and 1(b)) is realized when the rate of volumetric strain momentarily vanishes as the soil passes from the compressive mode of deformation to the dilatant mode of deformation during shearing. For a given cohesionless soil, these characteristic states generally depend upon the initial relative density, D_r, of the soil as well as the confining pressure under which the test is performed [1, 14, 16, 20, 21, 25]. When shearing occurs under a moderately high confining pressure, cohesionless soils often exhibit compressive volumetric response up to failure indicating merging of the two characteristic states (e. g., points 1′ and 2′ in Figs. 1(a) and 1(b)). This may also be true when a relatively loose soil undergoes shearing under moderately high confining pressure. With the exception of the

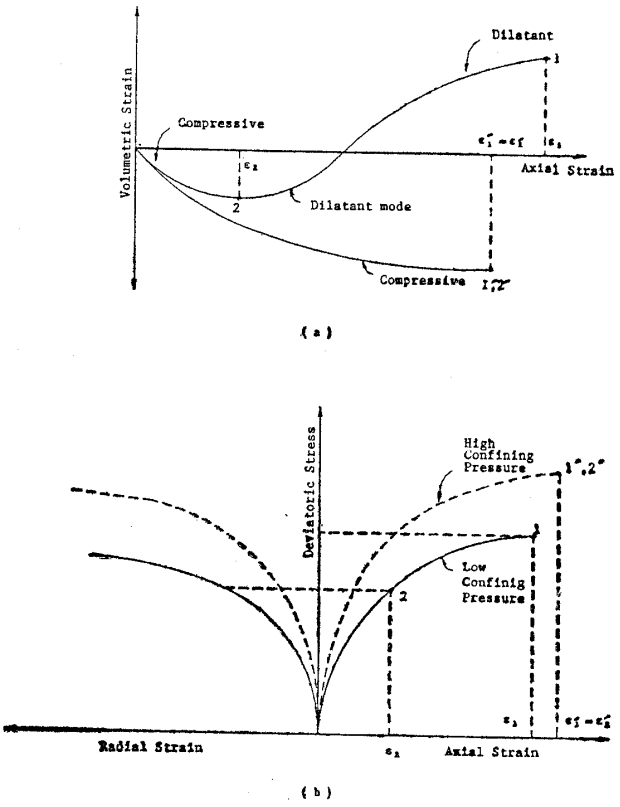

Fig. 1. Typical volumetric and axial response of cohesionless soil

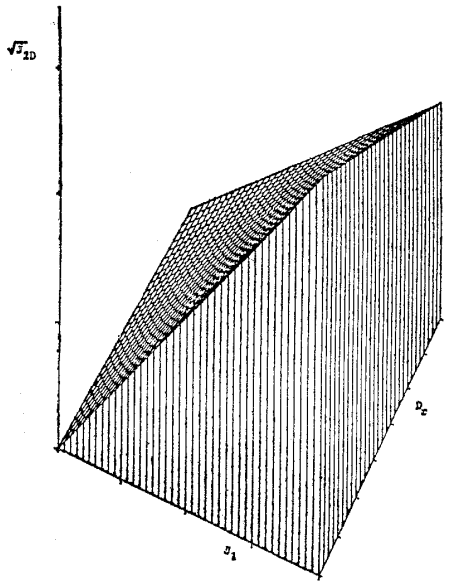

Fig. 2(a). Schematic representation of the first characteristic state surface in $J_1-\sqrt{J_{2D}}-D_r$ space

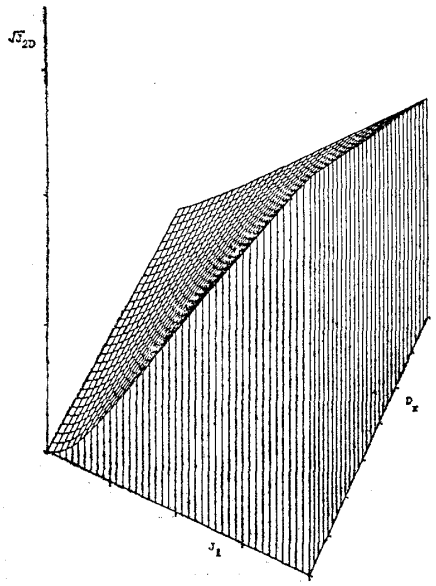

Fig. 2(b). **Schematic representation of the second characteristic state surface in $J_1-\sqrt{J_{2D}}-D_r$ space**

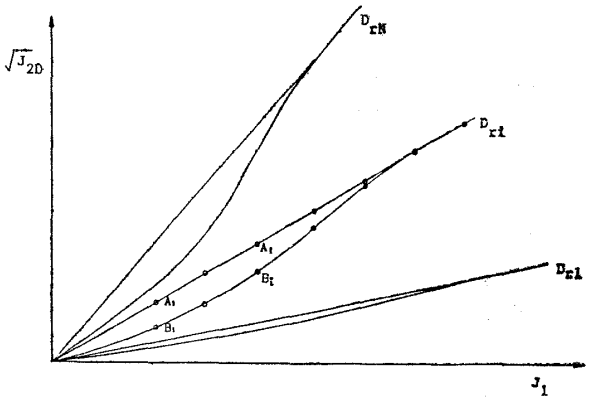

Fig. 3. **Schematic representation of the two characteristic state lines for various initial relative densities (D_{r1}, D_{ri}, D_{rN})**

above cases, the two characteristic states for a given cohesionless soil are distinct.

The characteristic states of a cohesionless soil can be represented in the form of characteristic state surfaces in the $J_1-\sqrt{J_{2D}}-D_r$ space as shown schematically in Figs. 2(a) and 2(b). The variables J_1 and $\sqrt{J_{2D}}$ denote the first invariant of the stress tensor and the second invariant of the deviatoric stress tensor, respectively. For a given initial relative density, the characteristic state surfaces degenerate to the characteristic state lines in the $J_1-\sqrt{J_{2D}}$ space. For various values of initial relative density, D_{ri} $(i=1, \ldots \overline{N})$, the characterisict state lines are shown schematically in Fig. 3. It is evident that the two characteristic state lines are distinct in most parts and tend to merge as the confining pressure becomes high. Also, the deviation of the characteristic state lines increases with the increase in initial relative density.

SOME SHORTCOMINGS OF THE EXISTING MODELS

There are some shortcomings of the existing plasticity based constitutive models for cohesionless soil in regard to characterization of dilatancy. This can be explained by using Fig. 4 which shows the typical elements of a cap type constitutive model [1, 6-12, 19, 20, 22, 27]. Typically the yield cap originates from J_1 axis and terminates at the failure envelope where the tangent to the yield cap is horizontal. As a result, within the framework of associative plasticity theory, only compressive volumetric strain will be obtained for stress states lying on the yield cap including point L (Fig. 4). Since the normal to the yield cap is vertical at point L, it represents the onset of dilatancy which corresponds to point 2 (i. e. the second characteristic state) in Fig. 1(a). However, point L also lies on the failure envelope which corresponds to point 1 (i. e. the first characteristic state) in Fig. 1(a). This is conceptually wrong because points 1 and 2 are distinctly different for cohesionless

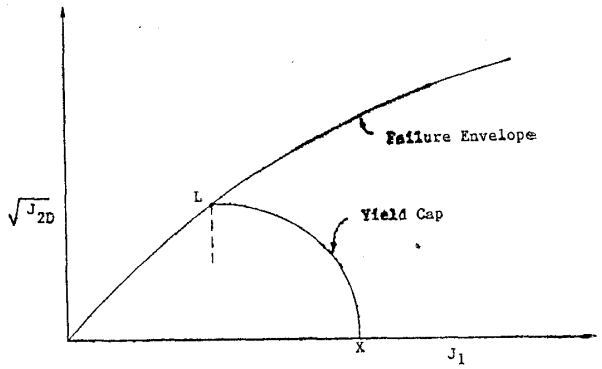

Fig. 4. **Elements of a typical cap type constitutive model**

soil under general conditions as evident from Fig. 1(a). An exception of this is possible when a cohesionless soil is subjected to high confining pressures where the two characteristic states merge as shown by points 1′ and 2′ in Fig. 1(a).

The constitutive models based on the non-associative plasticity theory [19, 20] also do not account for the second characteristic state in the formulation and therefore the onset of dilatancy and subsequent volumetric response cannot be predicted in a rational manner.

FORMULATION OF THE PROPOSED MODEL

First Characteristic State Line

Experimental observations have shown that the first characteristic state line (CSL-1) for cohesionless soil is an approximate straight line on the $J_1-\sqrt{J_{2D}}$ plane. This shows that the shear strength of such soil increases linearly with the confining pressure which is consistent with the Mohr-Coulomb theory of failure of granular soils. The slope of the characteristic state line (CSL-1) is a measure of the internal frictional coefficient and increases with increasing initial relative density, D_r, due to increasing compactness of the grains. Fig. 3 shows the plots of CSL-1 for a typical cohesionless soil at various initial relative densities.

For a given initial relative density, the first characteristic state line for cohesionless soil also depends upon the orientation (θ) of a stress path on the octahedral plane. A common definition of θ is given by

$$\theta=\frac{1}{3}\cos^{-1}\left[\frac{3\sqrt{3}\ J_{3D}}{2\ (J_{2D})^{3/2}}\right] \qquad (1)$$

where $J_{3D}=\frac{1}{3}\ S_{ij}\ S_{jk}\ S_{ki}$ is the third invariant of the deviatoric stress tensor (S_{ij}). The orientation θ lies in the range $0°\leq\theta\leq60°$, where $\theta=0°$ represents a compression stress path and $\theta=60°$ represents an extension stress path. As evident from experimental observations [1, 6, 12, 18], the slope of the first characteristic state line is maximum for $\theta=0°$ and minimum for $\theta=60°$.

In view of the above discussion, the equation of the first characteristic state line (CSL-1) can be written in the form

$$\sqrt{J_{2D}}=M\ g(\theta)\ J_1 \qquad (2)$$

where M is a material response function of the initial relative density, D_r and $g(\theta)$ is a function that accounts for the change in the slope of CSL-1 with θ. Following the works of Podgorski [24] and Faruque and Chang [11], $g(\theta)$ can be expressed as

$$g(\theta)=\cos\left[\frac{1}{3}\cos^{-1}\ (-A\ \cos\ 3\theta)\right] \qquad (3)$$

where A is assumed to be unity to satisfy convexity. Assuming M_o as the value of M at $D_r=0$ (i. e. loosest possible state), a functional form of $M(D_r)$ can be written as

$$M(D_r)=M_o\ [1+h_1(D_r)] \qquad (4)$$

in which $h_1(D_r)$ is a response function that determines the ratio M/M_o for a given initial relative density, D_r, and satisfies the condition $h_1(0)=0$. Note that $h_1(D_r)$ is a monotonically increasing function of D_r and attains maximum value at $D_r=1$ (i. e., densest possible state). Denoting the maximum value of $h_1(D_r)$ as λ_1, the following form of $h_1(D_r)$ is proposed

$$h_1(D_r)=\lambda_1\ D_r^{\eta_1} \qquad (5)$$

where the exponent η_1 signifies the shape of the function $h_1(D_r)$. In general, $h_1(D_r)$ can assume the representations shown by curves A, B and C in Fig. 5.

The rate of change of M with D_r (i. e.,

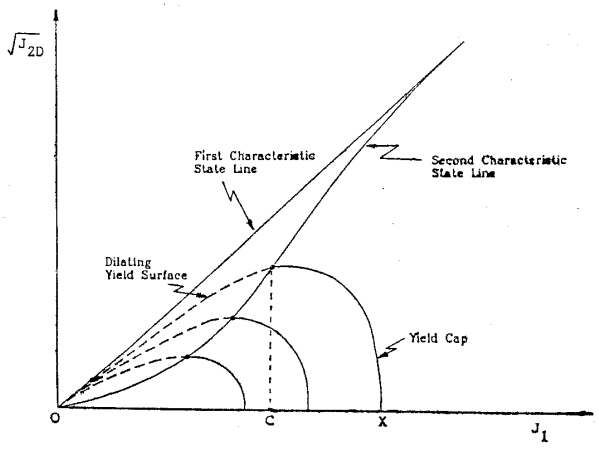

Fig. 5. Schematic representation of yield cap and dilating yield surface on $J_1-\sqrt{J_{2D}}$ space

dm/dD_r) generally decreases with increasing initial relative density. Therefore, curve A (Fig. 5) is an unlikely representation of $h_1(D_r)$. The proposed form of $h_1(D_r)$ in Eq. (5) can be validated using appropriate experimental data.

Second Characteristic State Line

Unlike the first characteristic state line (CSL -1), experimental observations as to the second characteristic state line is non-existent in the literature. It is, however, known that the second characteristic state tends to merge with the first characteristic state as the confining pressure becomes very high. As a result, the second characteristic state line should approach the first characteristic state line as the confining pressure increases. The proposed forms of CSL-2 on the $J_1-\sqrt{J_{2D}}$ plane for various initial relative densities are schematically shown in Fig. 3. For relatively loose cohesionless, soils, the characteristic state lines are quite close as indicted in Fig. 3. For higher initial relative density, the deviation of the characteristic state lines increases. Referring to Fig. 3, an equation of the second characteristic state line (CSL-2) is proposed in the form

$$\sqrt{J_{2D}}=M\left[1-N\cdot\exp\left(-\mu\cdot\frac{J_1}{P_a}\right)\right] g(\theta)\ J_1 \qquad (6)$$

where μ is a material constant, P_a is the atmospheric pressure expressed in the same unit as J_1 and N is a material response function of the initial relative density D_r. For high values of J_1, the exponential term in Eq. (6) becomes negligible and thereby, Eq. (6) approaches the first characteristic state line defined by Eq. (1). Referring to Eq. (6), the secant slope $(\sqrt{J_{2D}}/J_1)$ at $J_1=0$ is obtained as $M(1-N)\ g(\theta)$. Therefore, the material response function N determines the initial slope of the second characteristic state line at $J_1=0$. When $N=0$, both characteristic state lines have the same initial slope of M. Preliminary results on a beach sand [13] indicates that the initial slope of the second characteristic state line is smaller than M and in general, a function of the initial relative density, D_r. Assuming $N=N_o$ at $D_r=0$ (i. e., loosest possible state), a functional form of $N(D_r)$ can be written as

$$N(D_r)=N_o\ [1+h_2(D_r)] \qquad (7)$$

where $h_2(D_r)$ determines the ratio N/N_o for a given D_r and satisfies the condition $h_2(0)=0$. Following the analogy of $h_1(D_r)$, it is postulated that $h_2(D_r)$ is a monotonically increasing function of D_r and attains maximum value λ_2 at $D_r=1$ (i. e., densest possible state). In view of this, the following form of $h_2(D_r)$ is proposed

$$h_2(D_r)=\lambda_2 D_r^{\eta_2} \qquad (8)$$

The exponent η_2 in Eq. (8) dictates the shape of the function $h_2(D_r)$. The proposed form of $h_2(D_r)$ in Eq. (8) can be validated by using appropriate experimental data.

Compressive Yield Surface

Consistent with the definition of CSL-2, all states of stress below the second characteristic state line yield compressive volumetric strain only. Therefore, within the associative theory of plasticity, an yield surface between the J_1-axis and the second characteristic state line should be defined such that the normal to the yield surface at any point has non-negative slopes. Besides, the normal to the yield surface at the point of intersection with the second characteristic line (CSL-2) should be parallel to the $\sqrt{J_{2D}}-$axis. This is because, by definition, CSL-2 contains all stress states where the rate of volumetric deformation momentarily vanishes as the soil passes from the compressive mode of deformation to the dilatant mode of deformation during shearing. An elliptical yield surface that satisfies the above requirements is used in the proposed model and is shown schematically in Fig. 6. It is evident that the tangent to the yield surface at the intersection with J_1-axis is vertical. This insures purely spherical response under hydrostatic loading and is required for an isotropic material. An equation of the compressive yield surface is proposed as

$$F_c\equiv\sqrt{J_{2D}}-\sqrt{a^2-\frac{1}{R^2}(J_1-C)^2}\ g(\theta)=0 \qquad (9)$$

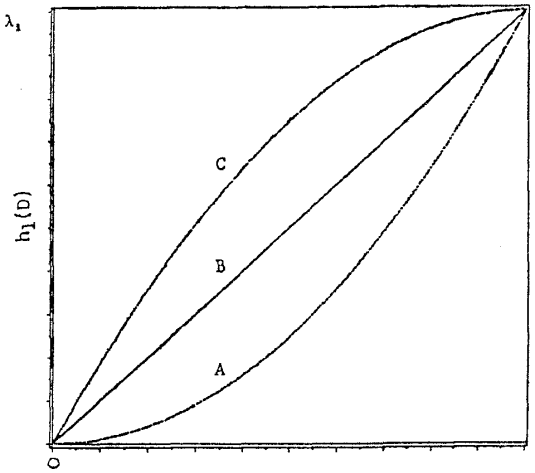

Fig. 6. Schematic representation of function $h_1(D)$

where R is a constant associated with the ratio of the axes of the ellipse and is a material constant and, in general, C is a response function that denotes the value of J_1 at the point of intersection of the yield surface and the second characteristic state line. In Eq. (9), a represents the axis of the elliptical yield surface parallel to $\sqrt{J_{2D}}$ axis and is defined in terms of C as

$$a=M[1-N\cdot\exp(-\mu\cdot C/P_a)]\ g(\theta)C \tag{10}$$

Note that elliptical yield surface has been used in other models such as cap model [1, 6-12, 19, 20, 22, 28] in the past and found to be satisfactory for the prediction of response in the compressive mode of deformation. However, other convex mathematical functions that satisfy the requirements of a yield surface discussed earlier may also be used.

The proposed model utilizes a nonassociative formulation to describe the volumetric response in the compressive regime. A plastic potential function, Q_c, is defined in the form

$$Q_c\equiv\sqrt{J_{2D}}-\bar{A}\sqrt{a^2-\frac{1}{R^2}(J_1-C)^2}\ g(\theta) \tag{11}$$

where $\bar{A}$ is a material constant. Taking the derivatives of F_c and Q_c with respect to J_1, the following relationship can be obtained

$$\frac{\partial Q_c}{\partial J_1}=\bar{A}\ \frac{\partial F_c}{\partial J_1} \tag{12}$$

As evident from Eq. (12), the constant $\bar{A}$ signifies deviation from normality and should have a positive value. The condition $\bar{A}>0$ is necessary to maintain compressive volumetric strain for stress states below CSL-2. For $\bar{A}=1$, $Q_c=F_c$, which represents associative formulation.

Dilating Yield Surface

By definition, a dilating yield surface refers to the stress states that cause dilating response at a material point. As described earlier, at a high confining pressure, cohesionless soil experiences compressive mode of deformation at all stages of loading up to failure. This indicates that the dilating yield surface is bounded by CSL-1 and CSL-2 at all times and identifies itself with the first characteristic state line (CSL-1) when the confining pressure is very high (Fig. 6). An equation of the dilating yield surface that satisfies the above requirements is proposed in the form

$$F_d=\sqrt{J_{2D}}-a\left[1-(1-J_1/C)^{\frac{MC}{a}}\right]g(\theta)=0 \tag{13}$$

A schematic representation of Eq. (13) is shown in Fig. 6. As evident, the tangent to the dilating yield surface at the point of intersection with the second characteristic state line is horizontal and thereby satisfies slope compatibility with the compressive yield surface, $F_c=0$. At $J_1=0$, the slope of the dilating yield surface is M and therefore, tangential to the first characteristic state line at that point.

It is evident from Fig. 6 that the normal to the dilating yield surface at any point has a non-positive slope which decreases with the stress state approaching the first characteristic state line. As a result, within the associative theory of plasticity, the model predicted rate of dilatancy increases continuously as the stress paths approach the first characteristic state line. This is contrary to the definition of CSL-1 that contains all stress states for which a soil experiences progressive shear deformation at constant volume (i. e., zero rate of dilatancy). It is, therefore, necessary to incorporate some mechanism in the model that will enable it to predict zero rate of di-

latancy when the stress state is on the characteristic state lines (both CSL-1 and CSL-2) and nonzero rate of dilatancy when the state of stress lies in between the characteristic state lines. In the proposed model, this is achieved by using non-associative formulation. To this end, a dilating potential function, Q_d, is defined by the following equations.

$$\frac{\partial Q_d}{\partial J_1}=q(J_1,\ J_{2D})\ \frac{\partial F_d}{\partial J_1} \tag{14}$$

$$\frac{\partial Q_d}{\partial J_{2D}}=\frac{\partial F_d}{\partial J_{2D}} \tag{15}$$

$$\frac{\partial Q_d}{\partial \theta}=\frac{\partial F_d}{\partial \theta} \tag{16}$$

where

$$q(J_1,\ J_{2D})=\alpha\frac{(\beta+\gamma)^{\beta+\gamma}}{\beta^{\beta}\gamma^{\gamma}}(1-G)^{\gamma}\ G^{\gamma} \tag{17}$$

in which

$$G(J_1,\ J_{2D})=\frac{MJ_1-\sqrt{J_{2D}}/g(\theta)}{MN\ \exp(-\mu J_1/P_a)J_1} \tag{18}$$

In above equations α, β and γ are material constants and the function $G(J_1, J_{2D})$ assumes a value of unity at CSL-2 and zero at CSL-1. Consequently, the function $q(J_1, J_{2D})$ becomes zero at the boundaries (CSL-2 and CSL-1) and is nonnegative elsewhere. $q(J_1, J_{2D})$ has a maximum value of α at $G(J_1, J_{2D})=\beta/(\beta+\gamma)$. Note that only derivatives of the potential function Q_d is required to obtain the elasto-plastic constitutive matrix. As such an explicit form of Q_d is not necessary.

Hardening Behavior

In this work, modeling of soil response under monotonic loading is attempted using the concept of isotropic hardening plasticity. Both the compressive yield surface, F_c, and the dilating yield surface, F_d, are allowed to expand in the stress space to account for stress states in the elasto-plastic regime. As discussed by many investigators in the past [8], hardening behavior of cohesionless soil is primarily attributed to irreversible (plastic) volumetric deformation. As such, history of inelastic volumetric strain is frequently used to describe hardening of cohesionless soil during hydrostatic loading as well as during shear loading. Commonly a hardening function is prescribed in terms of the accumulated plastic volumetric strain and the associated material constants are determined using hydrostatic compression test data only. It is important to realize that the mechanism of inelastic volume change during hydrostatic compression is quite different from that in shear. As a result, a hardening function, with its constants determined from hydrostatic compression test data, generally cannot describe elasto-plastic stress-strain and volumetric behavior during shearing in a rational manner. This problem can be resolved by expressing a hardening function in terms of two parameters, the total volumetric plastic strain, ξ_H, in the hydrostatic compression phase and an inelastic deformation measure, ξ_s, in shearing phase. The quantities ξ_H and ξ_s can be expressed in terms of the incremental plastic strain tensor, $d\varepsilon_{ij}^p$, as

$$\xi_H=\int d\varepsilon_{ij}^p\ \delta_{ij} \tag{19}$$

$$\xi_s=\int (d\varepsilon_{ij}^p\ d\varepsilon_{ij}^p)^{1/2} \tag{20}$$

where, δ_{ij} is the Kronecker delta and $\int$ denotes history. Note that ξ_s has zero value throughout hydrostatic compression. ξ_H, on the other hand, reaches its maximum value at the end of hydrostatic compression and remains constant throughout shearing.

Referring to Fig. 6, the compressive yield surface, F_c, originates from the J_1—axis (i. e. point X) and terminates at a point on the second characteristic state line (CSL-2) where J_1 assumes a value of C. The dilating yield surface, F_d, on the other hand, starts from the origin O and terminates at CSL-2 where $J_1=C$. As such, expansion of both F_c and F_d can be described conveniently by making C a (hardening) function of the parameters ξ_H and ξ_s.

For hydrostatic loading, C is a function of ξ_H only. To obtain an explicit form of $C(\xi_H)$, consider the representation of X in Fig. 6 (a point on the J_1—axis where the yield surface F_c originates) frequently used in the cap type models as

$$X=-\frac{1}{D}\ln\left[1-\frac{\xi_H}{W}\right] \tag{21}$$

where D and W are material constants. Physical meaning of these constants are well established and therefore, is not discussed here. Using the relationship, $X=(C+Ra)$, as indicated by Eq. (9), the following form of $C(\xi_H)$ is obtained

$$C=C(\xi_H)=-\frac{1}{D}\ln\left[1-\frac{\xi_H}{W}\right]-Ra \tag{22}$$

It should be noted that the function $C(\xi_H)$ attains a value of $\bar{C}$ at the end of hydrostatic loading and corresponds to $\xi_H=\bar{\xi}_H$. During shearing, evolution of the hardening function C is due to ξ_s only and therefore requires an additional representation.

An evolution equation for $C(\xi_s)$ in the shearing phase is proposed as

$$C=\bar{C}+\bar{D}\ln\left[1+\bar{W}\,\xi_s\right] \tag{23}$$

where $\bar{D}$ and $\bar{W}$ are material constants that describe hardening during shearing. Evaluation of the elasto-plastic cnostitutive relation matrix involves the derivatives of the hardening function C (Eqs. (22) and (23)) with respect to ξ_H and ξ_s rather than the function C itself. It is, therefore, important to maintain continuity of the derivatives $\frac{\partial C}{\partial \xi_H}$ and $\frac{\partial C}{\partial \xi_s}$ as the loading changes from hydrostatic to shear. Referring to Eqs. (22) and (23), the derivatives $\frac{\partial C}{\partial \xi_H}$ and $\frac{\partial C}{\partial \xi_s}$ can be written as

$$\frac{\partial C}{\partial \xi_H}=\frac{1}{D\left(1+R\frac{\partial a}{\partial c}\right)(W-\xi_H)} \tag{24}$$

$$\frac{\partial C}{\partial \xi_s}=\frac{\bar{D}\,\bar{W}}{(1+\bar{W}\,\xi_s)} \tag{25}$$

At the end of hydrostatic loading $\xi_H=\bar{\xi}_H$ and $\xi_s=0$ and the continuity condition requires that $\frac{\partial C}{\partial \xi_H}=\frac{\partial C}{\partial \xi_s}$. Using this condition, along with Eqs. (24) and (25), the following expression for $\bar{D}$ can be obtained

$$\bar{D}=\frac{1}{\bar{W}\,D\left(1+R\frac{\partial a}{\partial c}\Big|_{c=\bar{c}}\right)(W-\bar{\xi}_H)} \tag{26}$$

In view of Eq. (26), it is apparent that the hardening behavior in the shearing phase is described by $\bar{W}$ only. As the state of stress approaches CSL-1, the quantities ξ_s and C tend to be unbounded. This characteristic is reflected in the expression of C in Eq. (23).

ELASTO-PLASTIC CONSTITUTIVE RELATIONS

Using the concept of non-associative plasticity theory, incremental plastic strain tensor, $d\varepsilon_{ij}^p$, can be expressed as

$$d\varepsilon_{ij}^p=d\lambda\frac{\partial Q}{\partial \sigma_{ij}} \tag{27}$$

where Q is the plastic potential function and $d\lambda$ is an unknown scalar to be determined from the consistency condition of prager, $dF=0$, F being the yield function. Following the standard steps of the theory of plasticity, elasto-plastic constitutive relation tensor, C_{ijkl}^{ep} can be written as

$$C_{ijkl}^{ep}=C_{ijkl}^{e}-\frac{C_{ijuv}^{e}\frac{\partial F}{\partial \sigma_{uv}}\frac{\partial Q}{\partial \sigma_{mn}}C_{mnkl}^{e}}{\frac{\partial F}{\partial \sigma_{pq}}C_{pqrs}^{e}\frac{\partial Q}{\partial \sigma_{rs}}-A(\xi_H,\ \xi_s,\ \sigma_{rs})} \tag{28}$$

where C_{ijkl}^{e} is the elastic constitutive tensor and $A(\xi_H,\ \xi_s,\ \sigma_{ij})$ is a measure of plastic modulus involving derivatives of the yield function F with respect to ξ_H and ξ_s and derivative of the potential function Q with respect to σ_{ij}. Eq. (28) is valid in the compressive as well as dilative regimes of shear deformation provided Q is appropriately defined. In the compressive regime, $Q=Q_c$ (Eq. 11), while in the dilative regime $Q=Q_d$ ddefine implicitly by Eqs. 14-18.

APPLICATION

Drained shear test data [1] for a fine sand with an uniformity coefficient of 1.84 is used in this study to investigate the characteristic states and to verify the proposed constitutive

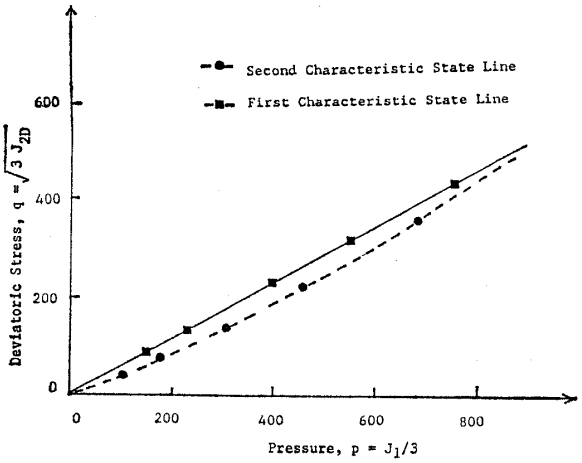

Fig. 7. The two characteristic state lines for a beach sand obtained from experimental data at 81 % initial relative density

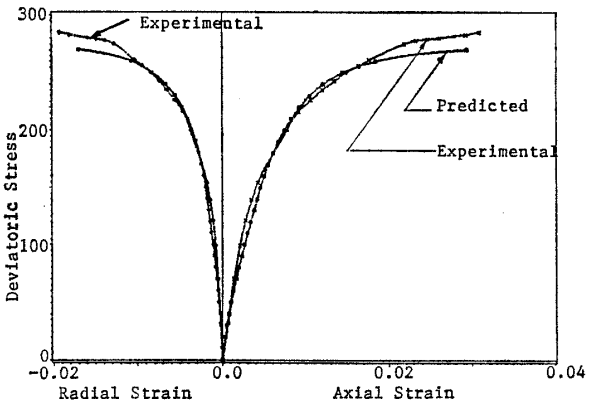

Fig. 8. Comparison of stress-strain response for conventional triaxial compression test

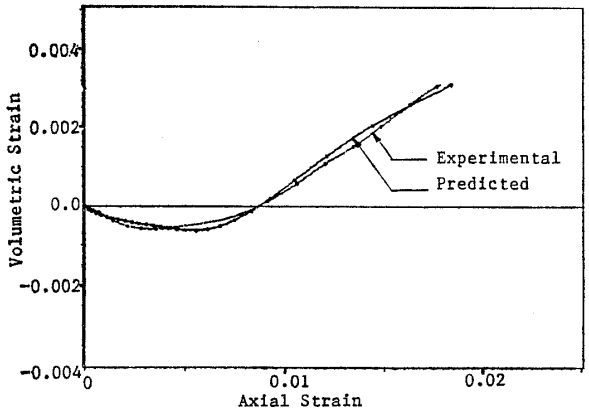

Fig. 9. Comparison of volumetric-axial strain response for conventional triaxial compression test

model. A stress controlled cylindrical triaxial device is used. The density of the test samples is in the range of 16.29 kN/m^3 to 16.59 kN/m^3 with an average relative densiy (D_r) of 81%. The characteristic state lines (CSL-1 and 2) obtained from the experimental data are depicted in Fig. 7. It is evident that the observed characteristic state lines are in agreement with the general forms proposed in the model. The second characteristic state line shows substantial deviation from CSL-1 in the low confining pressure range and tends to approach CSL-1 as the confining pressure becomes high.

Prediction of stress-strain response requires evaluation of material constants associated with the model. Since the tests are performed at a constant relative density (D_r=81%), only the following set of parameters are evaluated using a computer-aided complex optimization procedure [27] : K=130 MPa, G=70 MPa, M=0.27, N=0.44, μ=0.072, D=0.00087/KPa, W=0.0085, $\bar{W}$=1.0, R=2.5, $\bar{A}$=0.09, α=0.35, β=2.0 and γ=0.4.

Fig. 8 shows a comparison of the stress-strain response of a CTC (Conventional Triaxial Compression) test performed at a confining pressure of 104 KPa (15 psi). Evidently the model prediction is in excellent agreement with the experimental observation. A similar comparison of volumetric-axial strain response is shown in Fig. 9. It is observed that the proposed model is able to predict the onset of dilatancy and subsequent dilatant behavior in an accurate manner. The discrepancy between predicted and experimental axial strains at the onset of dilatancy (Fig. 9) can be attributed partly to error in measuring volumetric response using a burette. Detailed application of the proposed model is currently in progress and will be reported in subsequent papers.

CONCLUDING REMARKS

The concepts of two characteristic states and their representation as characteristic state lines in the stress space are introduced to describe volumetric behavior of cohesionless soil during shearing. The first characteristic

state line represents the state of cohesionless soil at failure, while the second characteristic line represents the state at which the rate of volumetric strain momentarily vanishes as the soil passes from the compressive mode of deformation to the dilative mode of deformation during shearing. Explicit forms of the two characteristic state lines in the stress space are proposed and used to develop a constitutive model based on the framework of plasticity theory. The general forms of the characteristic state lines are verified using drained shear test data for a fine sand. Stress–strain and volumetric–axial strain responses are predicted using the proposed model and good correlations are observed with experimental data.

REFERENCES

1) Abduljauwad, S. N., Faruque, M. O. and Azeemuddin, M. (1989): "Experimental verification and numerical evaluation of the three-invariant dependent cap model for cohesionless soil," paper submitted to *Computers and Geotechnics.*
2) Chang, C. S. (1985): "Dilatancy modelling for granular sand in simple shear condition," *Proc, 11th Int. Conf. on Soil Mech. and Found. Engrg.*, San Francisco, pp. 419–422.
3) Dafalias, Y. F. and Harrmann, L. R. (1982): "Bounding surface formulation of soil plasticity," Ch. 10, *Soil Mechanics-Transient and Cyclic Loads,* G. N. Pande and O. C. Zienkiewicz, (Eds.), pp. 253–282.
4) De Boer, R. (1988): "On plastic deformation of soils," *Int. J. of Plasticity,* Vol. 4, No. 4, pp. 371–391.
5) Desai, C. S. (1980): "A general basis for yield, failure and potential functions in plasticity," *Int. J. Numer. Anal. Methods Geomech.*, Vol. 4, pp. 361–375.
6) Desai, C. S. and Faruque, M. O. (1984): "constitutive model for (geological) materials," *Journal of Engineering Mechanics,* ASCE, Vol. 110, pp. 1391–1408.
7) Desai, C. S., Somasundaram, S. and Frantziskonis, G. (1986): "A hierarchical approach for constitutive modelling of geologic materials," *Int. J. Num. Analyt. Meth.* Geomech., Vol. 10, No. 3.
8) DiMaggio, F. L. and Sandler, I. S. (1971): "Material model for granular soils," *J. Eng. Mech. Div.*, ASCE, Vol. 97, No. EM 3, pp. 935–950.
9) Drucker, D. C., Gibson, R. E. and Henkel, D. J. (1957): "Soil mechanics and work hardening theories of plasticity," *Proc. ASCE,* Vol. 122, pp. 338–346.
10) Faruque, M. O. and Desai, C. S. (1985): "Implementation of a general constitutive model for geological materials," *Int. J. Num. Analyt. Meth. Geomech.*, Vol. 9, pp. 415–436.
11) Faruque, M. O. and Chang, C. J. (1986): "New cap model for failure and yielding of pressure sensitive materials," *J. Eng. Mech. Div.*, ASCE, Vol. 112, No. 10, pp. 1041–1053.
12) Faruque, M. O. (1987): "A third invariant dependent cap model for geological materials," *Soils and Foundations.* Vol. 27, No. 2, pp. 12–20.
13) Faruque, M. O. and Zaman, M. M. (1989): "Characteristic states experimental study and constitutive modeling of a beach sand," *Report,* School of Civil Engineering, University of Oklahoma.
14) Fukushima, S. and Tatsuoka, F. (1984): "Strength and deformation characteristics of saturated sand at extremely low pressures," *Soils and Foundations,* Vol. 24, No. 4, pp. 30–48.
15) Ghaboussi, J. and Momen, H. (1982): "Modelling and analysis of cyclic behavior of sand," *Soil Mechanics-Transient and Cyclic Loads,* G. N. Pande and O. C. Zienkiewicz, (Eds.), Wiley, Chpt. 12, pp. 313–342.
16) Hardin, B. O. (1988): "Low-stress dilation test," *J. Geotech. Eng.*, ASCE, Vol. 115, No. 6, pp. 769–787.
17) Hirai, H. (1987): "A Combined hardening model for plasticity for sands," *2nd Int. Conf. Short Course on Constitutive Laws for Engineering Materials: Theory and Applications,* C. S. Desai, et al. (Eds.), Elsevier, pp. 557–564.
18) Honarmandebrahimi, A. and Zaman, M. M. (1987): "Significance of testing procedure and equipment on determination of constitutive parameters for soil," *Proc Int. Conf. on Numerical Methods in Eng.: Theory and Applications,* held at Swansea, Vol. 2, pp. C 18/1–8.
19) Lade, P. V. and Duncan, J. M. (1976): "Elastoplastic stress-strain theory for cohesionless soil," *J. Geotech. Eng. Div.*, ASCE, Vol. 101, No. GT 10, pp. 1037–1053.
20) Lade, P. V. (1977): "Elastic-Plastic stress-strain

theory for cohesionless soil with curved yield surfaces," *International Journal of Solids and Structures,* Vol. 13, pp. 1019–1035.

21) Loung, M. P. (1980): "Stress–strain aspects of cohesionless soils under cyclic and transient loading," *Proc. Int. Symposium on Soils under Cyclic and Transient Loading,* G. N. Pande and O. C. Zienkiewicz (Eds.), Vol. 1, A. A. Balkema, Rotterdam, pp. 315–324.

22) Mroz, Z., Norris, V. A. and Zienkiewicz, O. C. (1978): "An anisotropic hardening model for soils and its application to cyclic loading," *Int. J. Numer. Anal. Methods Geomech.,* Vol. 2, pp. 203–221.

23) Mroz, Z. (1980): "On hypoelasticity and plasticity approaches to constitutive modelling of inelastic behaviour of soils," *Int. J. Numer. Anal. Methods Geomech.,* Vol. 4, No. 1, pp. 45–55.

24) Podgorski, J. (1985): "General failure criterion for isotropic media," *J. Eng. Mech.,* ASCE, 111, 188.

25) Pooroshasb, H. B. and Pietruszezak, S. (1985): "On yielding and flow of sand; A generalized two surface model," *Computer and Geotechnics,* Vol. 1, pp. 33–58.

26) Prevost, J. H. (1978): "Plasticity theory for soil stress–strain behavior," *J. Eng. Mech. Div.,* ASCE, Vol. 104, No. EM 5, pp. 1177–1194.

27) Relakitis, G. V., Revindran, A., and Ragsdell, K. M. (1983): "Engineering optimization methods and applications," John Wiley and Sons.

28) Sandler, I. S., DiMaggio, F. L. and Baladi, G. Y. (1976): "Generalized cap model for geological materials," *J. Geotech. Div.,* ASCE, Vol. 102, No. GT 7, pp. 683–699.

29) Valanis, K. C. and Read. H. E. (1982): "A new endochronic plasticity model for soils," Ch. 14, *Soil Mechanics-Transient and Cyclic Loads,* G. N. Pande and O. C. Zienkiewicz, (Eds.), pp. 375–468.

30) Zaman, M. M., Desai, C. S. and Faruque, M. O. (1982): "An algorithm for determining parameters for cap model from raw laboratory test data," *Proc. 4th Int. Conf. Numer. Methods Geomech.,* Edmonton, Canada.

31) Zienkiewicz, O. C., Humpheson, C. and Lewis, R. W. (1975): "Associated and nonassociated viscoplasticity and plasticity in soil mechanics," *Géotechnique,* Vol. 25, No. 4, pp. 671–689.